European Journal of Mechanics B/Fluids 28 (2009) 651–659

Contents lists available at ScienceDirect

European Journal of Mechanics B/Fluids

journal homepage: www.elsevier.com/locate/ejmflu

High Reynolds number gravity currents along V-shaped valleys

J.J. Monaghan [a], C.A. Mériaux [a,*,1], H.E. Huppert [b], J.M. Monaghan [a]

[a] School of Mathematical Sciences, Monash University, Victoria 3800, Australia
[b] Institute of Theoretical Geophysics, Department of Applied Mathematics and Theoretical Physics, University of Cambridge, CMS, Wilberforce Road, Cambridge CB3 0WA, UK

ARTICLE INFO

Article history:
Received 22 April 2008
Received in revised form
27 April 2009
Accepted 20 May 2009
Available online 28 May 2009

Keywords:
Gravity currents
Box model
Variable topography

ABSTRACT

The motion of saline gravity currents propagating horizontally in a tank of rectangular upper cross section and lower V-shaped valley is investigated both by lock-exchange experiments and a box model. The experiments were performed for equal depths of heavy and light fluid on both sides of the lock gate. The density ratio of the heavy fluid to the light fluid was in the range 1.04–1.13 and the lock height to length aspect ratios ranged from 0.5 to 1.6. We show that a box model with the Froude number of the head defined using the distance from the top of the current to the bottom of the valley predicts the position of the head in close agreement with the experiments. The presence of the valley results in three major differences in the gravity current compared to that flowing along a flat bottom. These are (a) the front of the current is approximately parabolic with radius of curvature proportional to the initial depth of the current, (b) for sufficiently large time t, the velocity of the current in the V-shaped valley varies as $t^{-1/5}$ compared to $t^{-1/3}$ in the flat bottom case, and (c) the width of the current in the V-shaped valley decreases with time t according to $t^{-2/5}$. Based on the box model, we predict that the steeper the flanks of the valley the faster the flow.

1. Introduction

Gravity currents are flows driven by a difference in density between the current and the ambient fluid into which it penetrates. They are widespread in nature (Simpson [1]). Gravity currents are affected by the bottom topography over which they flow, the entrainment of the ambient fluid and, in many cases, the particulate matter they carry. A comprehensive review and book by Simpson [1,2] describes much of the early work on gravity currents.

While most effort has been directed towards investigating such flows in flat-bottomed rectangular tanks, usually with homogeneous ambient fluids which are either initially at rest, or with a simple prescribed motion, there have been studies of gravity currents in other geometries. First constant volume gravity currents propagating at high Reynolds numbers down planar slopes (ramps) into a homogeneous fluid have been studied (see Ellison and Turner [3], Britter and Linden [4], Beghin et al. [5], Webber et al. [6]). These flows have shown characteristic differences from the horizontal gravity currents along flat-bottomed tanks both in the speed and form of the current (see for example the shadow photographs in Britter and Linden [4]). If the ramp flow is into a fluid stratified into two layers the complex phenomena that arise depend on the relative density of the current and the layers and depth of the layers (Monaghan et al. [7]). Waves may be generated [8] and the current can fill the upper layer, thereby making it continuously stratified, while not penetrating the lower layer (Wells and Wettlaufer [9]). In addition to studies of flows along planar surfaces horizontal or at an angle, Ross et al. [10] combined experiment and numerical simulations of the shallow water equations to study flows along cones (slope $< 5^\circ$) as a model of flow down a hill.

Flows of a single fluid along open channels of various shapes including in the shape of a V have commonly been reported in the hydraulics literature (see for example, [11]). Typically flows along these channels are considered to be fed by a constant flux, or discharge, rather than being that of a constant volume gravity current. For example, Antenucci et al. [12] have studied a constant flux flow along a V-shaped channel into a reservoir to model the spread of pathogens and constant flux currents along sinuous channels have been investigated using saline currents to model turbidity currents [13,14]. In addition, experiments relevant to oceanographic problems [15–18] make use of constant flux flows down channels and canyons in a rotating fluid system.

In this paper we consider gravity currents of both constant volume and high Reynolds numbers which flow along a tank which is a more realistic model of the valleys that occur in nature. This tank has a bottom that has the shape of a V and, above this valley,

* Corresponding author. Tel.: +61 3 9905 4404; fax: +61 3 9905 4403.
E-mail address: catherine.meriaux@sci.monash.edu.au (C.A. Mériaux).
[1] Departamento de Engenharia Geografic, Geofisica e Energia, Faculdade de Ciencas, Universidade de Lisboa, Campo Grande 1749-016 Lisboa, Portugal.

0997-7546/$ – see front matter © 2009 Elsevier Masson SAS. All rights reserved.
doi:10.1016/j.euromechflu.2009.05.005

has vertical side walls. As far as we are aware, there have been no studies of such gravity currents in a tank of the type we consider. We examine a series of 11 laboratory experiments involving turbulent currents with Reynolds numbers greater than 10,000. This study thus differs from those of Takagi and Huppert [19,20], which have studied flows along tanks of cross section in the shape of a V and more general shapes, but at low Reynolds numbers. In particular, in most of our experiments, the gravity currents undergo a transition from being above the V-shaped valley to being entirely within it.

One alternative to laboratory experiments is to accurately simulate the flows. The most accurate numerical simulation of our gravity current experiments would require a direct integration of the Navier Stokes equations. As the Reynolds dissipation length is $\Delta x = L(Re)^{-3/4}$, where L is a typical macroscopic scale of the flow, we can estimate that, for the problems we consider here, where the typical Reynolds number Re at the end of the experiments is 6000, $\Delta x \approx L/600$. This means that, disregarding details of the geometry of our tank, a direct numerical solution would require at least $L^3 \sim 2 \times 10^8 \Delta x^3$ cells to represent the domain. This estimate is greater than that used in the recent high resolution simulations of gravity currents in a flat-bottomed tank by Cantero et al. [21]. Note that an alternative to the direct numerical simulation would be to use a Large Eddy Simulation, or a model of the sub-grid dynamics. However, these would require elaborate testing for the specific geometry of our tank, in addition to very substantial computing resources.

The alternative we consider here is to explore approximate models which we justify *a posteriori* by their ability to predict the results of our experiments. The simplest of such models is a box model, which, in particular, does not explicitly take into account turbulence. This model cannot predict the details of the velocity field nor the waves at the interface between the current and the ambient fluid, but it can predict the speed and position of the head of the current. To characterize the speed of the current, we use a Froude number $Fr = U/\sqrt{g'h}$, where U is the current speed, g' is the reduced gravity and h is the depth of the current. This Froude number differs from the Froude number based on wave propagation in a fluid along a channel [11,22]. Different Froude conditions [23–27] have previously been proposed from theory and shown, in particular, to depend on the depth of the current relative to the total depth of the flow. For instance, von Kármán [23] was the first to show that $Fr = \sqrt{2}$ for a deeply submerged heavy fluid flowing into a semi-infinite lighter fluid, while Benjamin [24] showed that when the current occupied one-half the depth $Fr = 0.5$. Shin et al. [26] recently predicted that in a deep ambient fluid the Froude number is one. Based on lock-exchange experiments, Huppert and Simpson [25] reported a fit of their experiments in a rectangular tank with the empirical relation, $Fr = 1.19$ for h/H less than or equal to 0.075 and $Fr = 0.5(h/H)^{1/3}$ for h/H greater than 0.075, where h was the height of the current measured behind the head. This depth ratio dependence of the Froude number is much less for currents fed by a constant flux compared to fixed-volume currents released from a lock. The Froude number is then closer to $\sqrt{2}$ (See [1], Fig. 12.13). It is beyond the scope of this paper to study in detail the Froude condition for currents flowing in a rectangular tank with a V-shaped bottom. However we will show that a Froude number of 1 gives a good fit to our experiments.

In this paper, we first consider a similarity model for flow in a tank which has a cross section similar to our V-shaped valley. When this solution is compared with a box model we find the two approaches agree with errors of a few percent. We then work out the more general box model appropriate to our experiments and compare the results with the results of the experiments. The agreement is generally very good except for one experiment for which we will show that viscous effects became significant.

2. Laboratory experiments

2.1. Experimental setup and procedure

Fig. 1 shows the polycarbonate tank with its V-shaped bottom. The dimensions of the tank are inside width $W = 0.28$ m with vertical wall 0.40 m high and has a total length 5 m. The depth of the valley a measured vertically from the lowest point to the bottom of the vertical walls is 0.065 m. The slope of the valley is 25° to the horizontal. A lock gate is used to isolate a lock from the rest of the tank at a fixed distance $L = 0.13$ m from one end of the tank.

The tank was initially filled with fresh water while the lock was filled with a more dense fluid, in this case an aqueous saline solution. Both the tank and the lock were filled to a fixed depth H_0 measured from the water surface to the top edge of the valley (see Fig. 1). The saline fluid in the lock was dyed to visualize the currents on videos. Each experiment was initiated by rapidly lifting the gate.

The currents were filmed against a background grid of squares to determine the speed of the current from video films, as seen clearly in Fig. 2. The squares have side length 2.5 cm. The video film generates a frame every 0.04 s, which is sufficiently accurate for these experiments where the typical time for the current to reach 2 m is 7 s. A mirror was placed above the tank at a 45° angle to enable the current to be filmed from above at the same time as it was filmed from the side. Because the fluid in the V-shaped valley is at an angle to the line of sight of the camera, images of the current seen from the side can appear distorted when they are below the edge of the valley. However, images taken from above, which provide the data we discuss in this paper, are unaffected by the distortion. Table 1 gives the parameters of the experiments.

Eleven experiments (see Table 1) were performed. In the first nine experiments, saline solutions of densities $\rho_c = 1040$, 1080, and 1130 kg/m^3 were released into ambient fresh water of density $\rho_a = 1000$ kg/m^3 at successive heights $H_0 = 0.145$, 0.065 and 0 m. The density ratios defined by the ratio of the heavy fluid over the light fluid were thus in the range 1.04–1.13. In experiments 10 and 11, the saline solutions had a fixed density of $\rho_c = 1080$ kg/m^3 and H_0 was respectively 0 and 0.035 m. The Reynolds number of each current, which estimate is based on H_0, are high (see Table 1) and indicates the currents were turbulent. In experiments 1–9, the front of the currents was measured over a distance of 2 m from the video films. In experiments 10 and 11 the position of the front was measured over 2 m from the video film and beyond

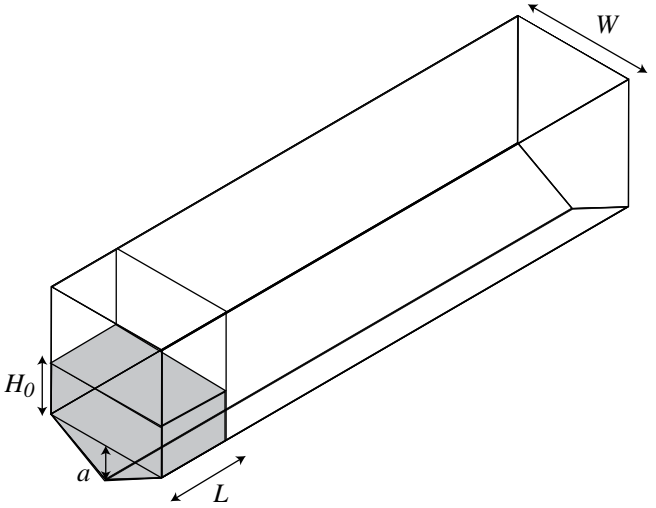

Fig. 1. Geometry of the V-shaped valley tank.

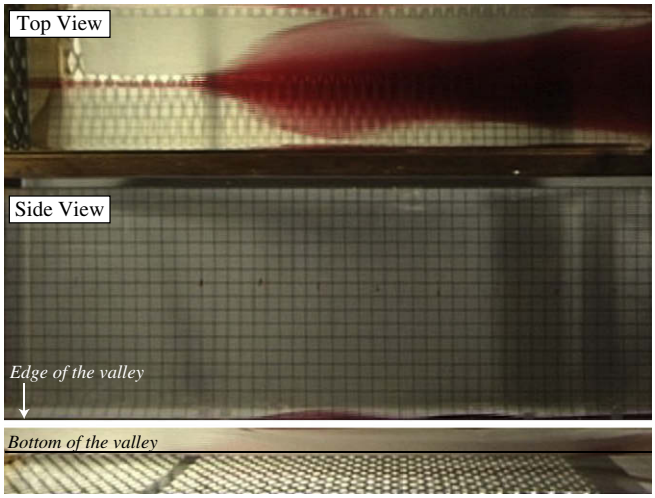

Fig. 2. The water from the lock shown red exiting into an empty tank. The initial depth of water above the valley was $H_0 = 0.145$ m, corresponding to a Reynolds number $Re_0 = \sqrt{g(H_0+a)^3}/\nu 2 = 3\times 10^5$. Note the head and neck as seen in the 45° mirror in the upper part and the side view of the rounded head, part of which can be seen in the lower part of the photograph rising above the edge of the valley. The valley is covered to prevent unwanted shadows.

(up to a distance of 5 m) by recording the time the front reached specified positions in the tank.

2.2. Flow regimes

2.2.1. Flow with no ambient fluid

Before describing the experiments it is interesting to show the flow of water from the lock into air and compare it to flow from a lock when the bottom is flat. In the latter case (often called a dam break), the fluid flows out as a nearly two dimensional flow with a rippled, but essentially straight front perpendicular to the flow direction and height which gradually increases towards the lock [28]. By contrast the flow in the V-shaped valley has a great deal of structure, as shown in Fig. 2. The fluid emerges and forms a front which is close to triangular with stream lines directed inwards towards the lowest point of the valley. This quickly evolves to form a more complex shape which, seen from above, has a neck and a rounded head. The valley thus has a profound effect on the flow.

Table 1
Experimental and scaling parameters. $\Delta\rho/\rho_a$ is the ratio of the density difference between the gravity currents ρ_c and ambient fluid ρ_a relative to ρ_a. ℓ and σ are respectively the length and time scales defined for the box model of Section 4. The initial Reynolds number Re_0 is estimated by using $Re_0 = \sqrt{g'(H_0+a)^3}/\nu^2$, where ν is the kinematic viscosity of water. Towards the end of the experiments the Reynolds number Re is calculated as $\dot{X}h/\nu$, where $\dot{X}$ is the velocity of the head of the current estimated over the last half of each experiment and the depth of current h at the final position of the head in Figs. 5–9. The long run experiments 10 and 11 have small Reynolds numbers at the end of the run.

Exp.	H_0	$\Delta\rho/\rho_a$	ℓ	σ	Re_0	$\dot{X}$	Re
1	0.145	0.04	0.71	6.3	60,283	0.17	7600
2	0.145	0.08	0.71	4.5	85,253	0.24	10,000
3	0.145	0.13	0.71	3.5	108,676	0.30	13,000
4	0.065	0.04	0.39	3.5	29,362	0.14	4900
5	0.065	0.08	0.39	2.4	41,523	0.19	6700
6	0.065	0.13	0.39	1.9	52,932	0.25	8800
7	0.000	0.04	0.13	1.2	10,380	0.09	2000
8	0.000	0.08	0.13	0.81	14,680	0.12	2400
9	0.000	0.13	0.13	0.64	18,714	0.17	3400
10	0.000	0.08	0.13	0.81	14,680	0.12	~ 1
11	0.035	0.08	0.27	1.69	28,014	0.19	~ 1

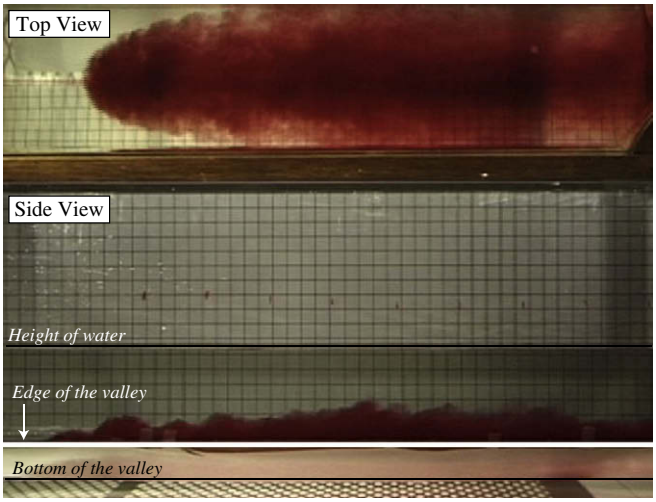

Fig. 3. The gravity current in experiment 3 (see Table 1) seen from above and from the side for the case. Note the rounded shape of the head, the ripples due to waves running from the head to the sides, and the disordered state of the top of the current seen from the side in the lower part of the figure. The current is thinner at the sides because of the valley.

2.2.2. Flow with ambient fluid

Fig. 3 shows a typical current seen from above for the case where $H_0 = 0.145$ m. The points to note are: first the curved head; second the ripples around the side of the head (presumably Kelvin Helmholtz instabilities); and third the fact that the current is thinner on the sides of the valley (shown by the lighter shade of red). The lower part of the figure shows the disorder of the top of the current and the absence of a dominant head when seen from the side.

Fig. 4 shows a typical current from above for the case where $H_0 = 0$ m so that the initial surface of the fluid is leveled with the edge of the valley and subsequently remains within it. The head is curved as before, but the radius of curvature is smaller than in Fig. 4. Waves ripple the side of the head as in the previous case, but the wavelength is less.

2.2.3. Parabolic front of the currents

Both for currents flowing at all times within the valley, as shown in Fig. 5, and for currents flowing initially above the valley and then

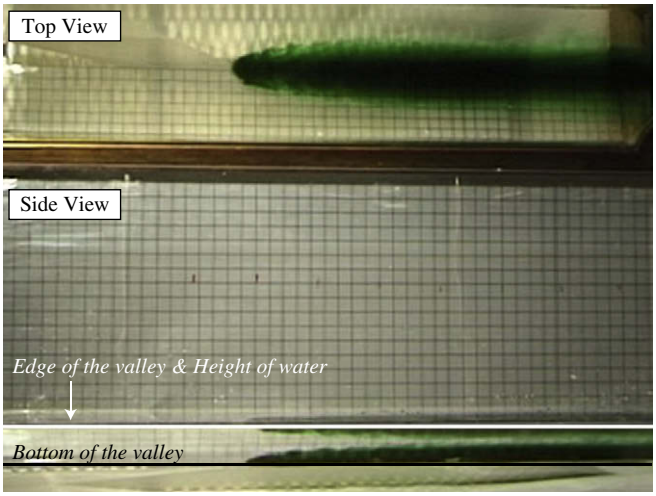

Fig. 4. The gravity current in experiment 8 (see Table 1) seen from above for the case. Note that the head is smaller than in the previous figure, and the radius of curvature of the head is correspondingly smaller.

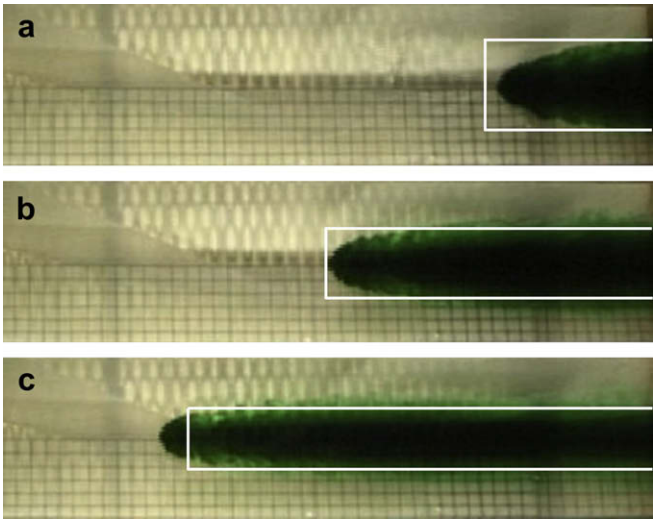

Fig. 5. The gravity current of experiment 8 seen from above at $t = 2.56$ (top frame a), 4.92 (middle frame b) and 6.96 s (bottom frame c) after the opening of the lock gate. The white lines show the boundaries of the box model.

entirely within the valley, as shown in Fig. 6, the shape of the fronts appears to be parabolic. As H_0 is reduced, the radius of curvature R of the head decreases. R can be estimated using Newton's method which is based on the fact that R is the radius of curvature of a circle which can be fitted with the profile of the current in the neighborhood of that part of the head which is furtherest along the tank. We define this circle by $(x' - R)^2 + y'^2 = R^2$, where (x', y') defines a system of local coordinates whose origin is the point of the current at the furthest distance from the lock. x' is measured from the vertex towards the lock, and y' is measured from the centerline to the edge of the current. For $x' \ll R$, the equation of the circle can be approximated to give $R = (y')^2/(2x')$. By measuring a set of (x', y') on the edge of the current in the neighborhood of its head R can be estimated. In practice this procedure is complicated because of the ripples around the head. For this reason two of us independently measured the values of x', y' and the average was used. The measurements were repeated for different flow times for each gravity current.

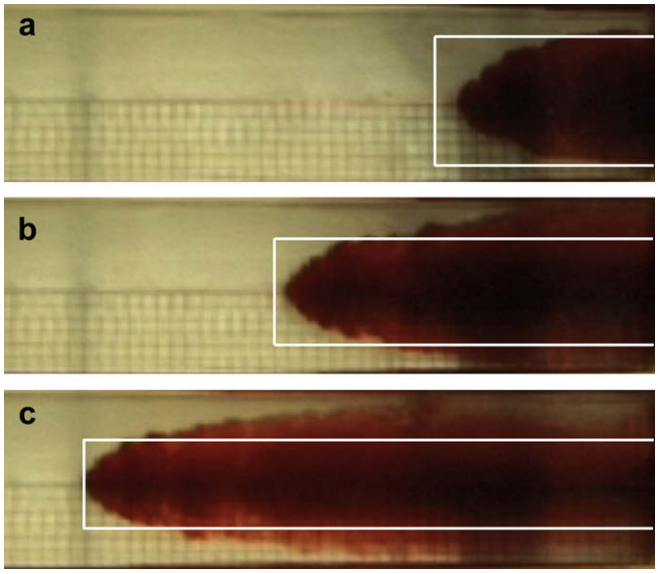

Fig. 6. The gravity current of experiment 5 seen from above at $t = 2.24$ (top frame a), 3.76 (middle frame b) and 5.60 s (bottom frame c) after the opening of the lock gate. The white lines show the boundaries of the box model.

Consistent with dimensional analysis, R was found to have the following linear variation with initial fluid height above the bottom of the valley

$$R = b(H_0 + a), \tag{1}$$

where $b = 0.23 \pm 0.03$. This estimate is only approximate because the surface of the head is rippled. Remarkably, for all the currents we studied, the radius of curvature remains nearly constant as shown by Figs. 5 and 6.

3. Analytic solutions for gravity currents flowing entirely within a valley

In this section we consider a similarity model for a flow within a V-shaped valley. When this solution is compared with the one of a box model based on the geometry, we show that the two approaches estimate a speed of the front of the current which differ by at most a few percent.

3.1. Similarity solution

Here we present a similarity solution for the case of a gravity current flowing along a tank with width w defined by

$$w = W(z/D)^{\alpha}, \tag{2}$$

where $\alpha \geq 0$ is a constant, the height z is measured from the bottom of the valley and D is the length scale for the depth of the valley. It is assumed that there is no mixing between the gravity current and the ambient fluid.

The derivation of the similarity solution follows a standard procedure [29] for which we give the main steps.

We define the similarity variable $\eta = x/X$, where $X(t)$ is the length of the current. The height and velocity of the current are defined by

$$h(x,t) = h_f(t)H(\eta) \text{ with } H(1) = 1,$$

$$u(x,t) = u_f(t)U(\eta) \text{ with } U(1) = 1.$$

The cross-sectional area can be written

$$A = \int_0^h w dz = Bh^{\alpha+1}, \tag{3}$$

where $B = W/(D^{\alpha}(\alpha+1))$, and the volume of the current V is given by

$$V = \int_0^X A dx = Bh_f^{\alpha+1} X \int_0^1 H(\eta)^{\alpha+1} d\eta. \tag{4}$$

Assuming that the volume of the current is constant, we deduce that $Xh_f^{\alpha+1}$ is constant. Substituting these expressions into the continuity equation

$$\frac{\partial A}{\partial t} + \frac{\partial}{\partial x}(uA) = 0, \tag{5}$$

gives a non trivial solution $U(\eta) = \eta$.

The momentum equation takes the form

$$\frac{\partial u}{\partial t} + u\frac{\partial u}{\partial x} + g'\frac{\partial h}{\partial x} = 0, \tag{6}$$

where g' is the effective gravity defined by $g' = g|\rho_c - \rho_a|/\rho_a$. Substituting the previous expressions into the momentum equation, and using the Froude number condition at the front of the current

$$\frac{dX}{dt} = Fr\sqrt{g' h_f}, \tag{7}$$

where the Froude number Fr is assumed to be constant, we find

$$H(\eta) = 1 - \frac{Fr^2(1-\eta^2)}{4(\alpha+1)}, \tag{8}$$

which, when $\alpha = 0$, agrees with equation (14) of [30], if account is taken of their scaling which introduces a factor $1/Fr^2$. We note that the gravity current Froude condition of Eq. (7) has to be distinguished from the ratio of the gravity-current front speed to the linear long-wave speed defined by $Fr = U/c$, where c is the long-wave speed (for further discussion, see [22]).

With H a known function of η, we can substitute into Eq. (4) to get h_f in terms of X and other constant quantities. In general the integration requires numerical methods, but in the case where $\alpha = 1$, we find

$$V = BXh_f^2\left(1 - \frac{Fr^2}{6} + \frac{Fr^4}{120}\right), \tag{9}$$

and $B = W/2D$. Hence, by integrating Eq. (7), we get

$$X(t)^{5/4} = X(0)^{5/4} + t\left(\frac{5Fr}{4}\right)\left(\frac{2g'^2VD}{W(1 - Fr^2/6 + Fr^4/120)}\right)^{1/4}, \tag{10}$$

where $X(0)$ is the initial value of X. In our experiments, $Fr \sim 1$ as shown in Figs. 7, 8 and 9. We can thus approximate the term involving Fr in the denominator by 1. If t is sufficiently small we can approximate Eq. (10) by

$$X(t) \approx X(0) + \frac{tFr}{X(0)^{5/4}}\left(\frac{2g'^2VD}{W}\right)^{\frac{1}{4}}, \tag{11}$$

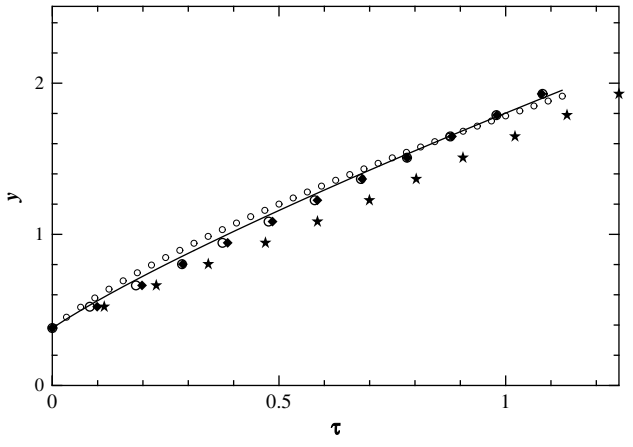

Fig. 7. The non-dimensional position of the head of the gravity current against non-dimensional time for the case where $H_0 = 0.145$ m. The experimental results for the density ratios of 1.04, 1.08, and 1.13 are shown by the large open circles, the filled squares, and stars respectively. The experimental results for density ratios 1.04 and 1.08 are close both to each other and a straight line. The continuous line shows the results from the box model using h with $Fr = 1.0$. The small open circles show the results using $\overline{h}$ with $Fr^* = 1.0$.

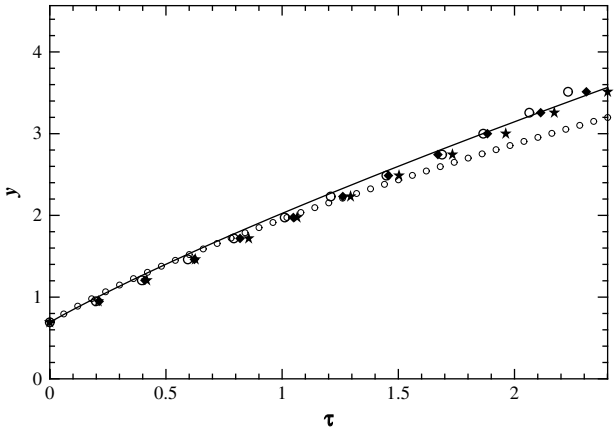

Fig. 8. The non-dimensional position of the head of the gravity current against non-dimensional time for the case where $H_0 = 0.065$ m. The experimental results for the density ratios of 1.04, 1.08, and 1.13 are shown by the large open circles, the filled squares, and stars respectively. The box models use $Fr = 0.9$ and $Fr^* = 1.1$. The continuous line shows the results from the box model using h with $Fr = 1.0$. The small open circles show the results using $\overline{h}$ with $Fr^* = 1.0$. The agreement between the experimental results and the box model using h is very good.

and when t is sufficiently large the $X(0)$ term can be ignored in (10) giving

$$X(t) \approx \left(\frac{5Fr}{4}\right)^{4/5}\left(\frac{2g'^2VD}{W}\right)^{\frac{1}{5}} t^{4/5}. \tag{12}$$

We note that we do not expect the similarity solution Eq. (11) to hold for short times.

An obvious but significant feature of the flow along the valley is that the current narrows with time. When $\alpha = 1$, the width of the current w can be estimated from h_f noting that $1/2wh_fX(t) = V$ which, combined with the expression for B given after Eq. (9) gives

$$w = \sqrt{\frac{2VW}{DX}}\left(1 - \frac{Fr^2}{6} + \frac{Fr^4}{120}\right)^{1/2} \propto \frac{1}{t^{2/5}}. \tag{13}$$

This time dependency of the width with time is in close agreement with the experiments. For example, the width of the boxes calculated with the box model in the three frames of Fig. 6 are 23.6 cm, 19.4 cm and 16.6 cm at times 2.32, 3.84 and 5.68 s respectively. If

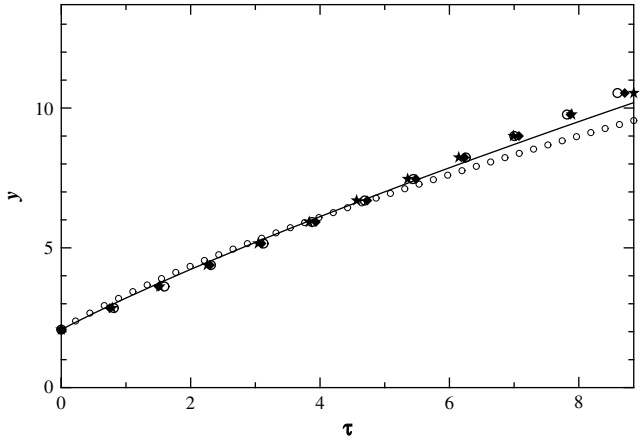

Fig. 9. The non-dimensional position of the head of the gravity current against non-dimensional time for the case where $H_0 = 0$ m. The notation is the same as in Figs. 7 and 8. The agreement between the experimental results and those from the box model using h is very good. The box model using $\overline{h}$ gives less satisfactory results. The box models use $Fr = 0.9$ and $Fr^* = 1.4$.

we use the width $w = 21.6$ cm at time 2.32 s and Eq. (13) to extrapolate the widths at time 3.84 s and 5.68 s, we get the corresponding widths of 19.3 cm and 16.5 cm.

If we compare with a flow within a channel of rectangular cross section with width W and the same volume V of fluid, the similarity solution is

$$X(t)^{3/2} = X(0)^{3/2} + t\left(\frac{3Fr}{2}\right)\left(\frac{g'V}{W(1 - Fr^2/6)}\right)^{1/2}, \tag{14}$$

and for sufficiently large t, and $Fr \sim 1$

$$X(t) \approx \left(\frac{3Fr}{2}\right)^{2/3}\left(\frac{g'V}{W}\right)^{\frac{1}{3}} t^{2/3}. \tag{15}$$

The difference between the solutions for flow along a tank with V-shaped or rectangular cross section is that the power of t is 4/5 in the first case and 2/3 in the second so the current in the V-shaped valley travels faster than in the rectangular valley of the same width for sufficiently large t.

3.2. A box model

The above similarity solution for the particulate shape given by Eq. (2) can be compared with the solution from a box model. Box models are based on a description of the flow, in which the properties of the current are assumed to be horizontally uniform. This implies that (1) the current has a uniform height and width and (2) the current is well mixed within its interior and there is negligible mixing between the current and the ambient fluid. The first assumption is equivalent to using the approximation $H(\eta) = 1$ for all η which, as seen from Eq. (8), is in error by $\sim 10\%$ when $\alpha \sim 1$. The second assumption is that mixing with the ambient fluid can be neglected, as in the case of the similarity solution discussed above. This assumption implies that V is constant. These assumptions will *a posteriori* be justified by the agreement with the experiments.

The Froude condition is given by

$$\frac{dX}{dt} = Fr\sqrt{g'h}. \tag{16}$$

For the case $\alpha = 1$, h can be written in terms of X using $V = BXh^2$. If this is substituted into Eq. (16), and the resulting equation integrated, we recover Eq. (10), with the factor $(1 - Fr^2/6 + Fr^4/120)$ replaced by 1.

Therefore, for a gravity current flowing entirely within a V-shaped valley, the box model predicts the position of the head in close agreement to the similarity solution. In our experiments, the cross section of the valley is not of the form given by Eq. (2). The current can be initially in contact with the vertical walls then eventually flows within the V-shaped valley. This transition introduces another length scale which greatly complicates any useful approximate solution other than the box model.

4. Numerical simulations of the experiments based on a box model

Having established that the box model is *a priori* a reasonable approach in the case of a flow within only a V-shaped valley, we present in this section the more general box model appropriate to our experiments and compare the results with the results of the experiments. We show that the box model can be justified *a posteriori* by its good agreement with the experimental results except for one experiment for which we will show that viscous effects became significant.

We consider two choices for the characteristic length scale used in the equation for dX/dt. The natural choice is to use $h(t)$, the depth of the fluid, but we also consider a second possibility with the average height $\overline{h}$, defined by $V = WX\overline{h}$. We note that we could have chosen the hydraulic depth $h_d = A/(\partial A/\partial h) = A(h)/B(h)$, which is related to h by $h_d = h - a/2$ when $h > a$ and $h_d = h/2$ when $h < a$. Referring to Fig. 1

$$V = LW\left(H_0 + \frac{1}{2}a\right). \tag{17}$$

During the flow the total volume is conserved and, when $h > a$ it can be written

$$V = XW\left(h - \frac{1}{2}a\right), \tag{18}$$

and when $h < a$ it can be written

$$V = \frac{Xh^2W}{2a}. \tag{19}$$

We first consider the case where $h > a$. From Eq. (18)

$$h = \frac{1}{2}a + \frac{V}{XW}. \tag{20}$$

Accordingly, while $h \geq a$, the equation of motion for X is

$$\frac{dX}{dt} = Fr\left[g'\left(\frac{1}{2}a + \frac{V}{XW}\right)\right]^{1/2}. \tag{21}$$

Using non-dimensional variables $y = X/\ell$ and $\tau = t/\sigma$ where

$$\ell = \left(\frac{2V}{aW}\right), \quad \sigma = \frac{\ell}{Fr}\sqrt{\frac{2}{g'a}}, \tag{22}$$

Eq. (21) becomes

$$\frac{dy}{d\tau} = \left(1 + \frac{1}{y}\right)^{1/2}, \tag{23}$$

which analytic solution is

$$y^{1/2}(1+y)^{1/2} - \ln\left(y^{1/2} + \sqrt{1+y}\right) = \tau + c_1, \tag{24}$$

where the constant c_1 is determined by the initial value of y.

Equation (23) only applies while $h \geq a$. When $h = a$, Eq. (20) shows that $X = \ell$ and therefore $y = 1$. After this point the gravity current is entirely in the valley and the volume of the gravity current is given by Eq. (15). The equation of motion then becomes

$$\frac{dX}{dt} = Fr\left(\frac{2ag'^2V}{XW}\right)^{1/4}, \tag{25}$$

which, with the previous scaling, becomes

$$\frac{dy}{d\tau} = \frac{\sqrt{2}}{y^{1/4}}. \tag{26}$$

Equation (26) has the solution

$$\frac{4}{5}y^{5/4} = \sqrt{2}\tau + c_2, \tag{27}$$

where c_2 is determined by requiring continuity of y at $y = 1$. At this point the velocity of the head is also continuous.

Using the scaling in Eq. (22), we rewrite Eq. (16), with $\overline{h}$ replacing h, as

$$\frac{dy}{d\tau} = Fr^*\frac{\sqrt{2}}{y^{1/2}}, \tag{28}$$

where Fr^* is the ratio of the Fr for the case where $\overline{h}$ is used to that with h. We expect, other things being equal, that Fr^* should be greater than 1 because $\overline{h} < h$.

Rather than using the analytical solutions, it is easier to integrate the equations numerically switching from Eq. (23) to Eq. (26) when $y = 1$. The values of Fr and Fr^* were adjusted to give a best fit to the experimental results. This was done by trial and error and the values of Fr are within 0.05 of the optimum values.

To complete our discussion of box models we briefly consider the general case where the breadth of the tank for any water height is $B(h)$. The cross-sectional area is then given by

$$A(h) = \int_0^h B(h')\,dh', \tag{29}$$

and because the volume $V = XA(h)$ is constant we can differentiate V with respect to time to deduce

$$\frac{dh}{dt} = -\frac{A}{B(h)X}\frac{\mathrm{d}X}{\mathrm{d}t}. \tag{30}$$

Making use of Eq. (16), Eq. (30) can be written

$$\frac{dh}{dt} = -\frac{VFr}{B(h)X^2}\sqrt{g'h}. \tag{31}$$

The system is then described by the two differential equations for the variation of X and h with time Eqs. (16) and (31).

5. Quantitative comparison between the experiments and the box model

5.1. Experiments with negligible viscous effects

In experiments 1–9, the measurements of the position of the front as a function of time were made from the video. These runs were typically measured over a length of 1.3 m. Over this length, the viscous effects were negligible.

The results are shown in Figs. 7 (for the case $H_0 = 0.145$ m) and 8 (for the case $H_0 = 0.065$ m) and 9 (for $H_0 = 0$ m). The experimental values of X were measured at the same grid points for all densities, but the values of y vary because the length scale varies with volume and therefore H_0. The experimental data were measured in that length of the tank (1.3 m) which was in the field of view of the video camera. The time scale changes with both volume and density ratio. For all these experiments, clock time commenced when $X = 0.27$ m. Note that $y = 1$ corresponds to the gravity current changing from being above to being below the edge of the V-shaped valley. Using Eq. (22) the value of X at this point is $\ell = 2V/(aW)$ which varies from 1 to ∼5.5 lock lengths L (see Table 1).

Fig. 7 shows the evolution of y with τ for the case where $H_0 = 0.145$ m. In this case the initial value of $y = 0.4$. The scaled experimental results for density ratios of 1.04, and 1.08 are very close to each other and both fit a straight line which differs only slightly from the box model results whether calculated using equations h, or using $\overline{h}$. The higher density ratio of 1.13 differs from the other two. In this case the values of y are less for a given τ, and show a change of slope at $\tau \sim 0.4$. The box models use $Fr = 1.0$ and $Fr^* = 1.0$. It can be seen from Fig. 7 that except for the density ratio 1.13, the values of y from the box model using h are initially above the experimental values, then drop below them. This trend is also evident in Figs. 8 and 9. The deviation from the model using $\overline{h}$ is greater than that using h.

Fig. 8 shows the evolution of y with τ for the case $H_0 = 0.065$ m. In this case the experimental results for all three density ratios are similar, with differences of ∼7% in the values of τ for a given y. The agreement with the box model results using h is very good. The box model results using $\overline{h}$ deviate significantly from the experimental results for $y > 2.6$ with good agreement for smaller values of y. The box models use $Fr = 0.9$ and $Fr^* = 1.1$.

Fig. 9 shows the evolution of y with τ when H_0 is zero. In this case the current is always in the valley. The experiments, and the box model results using h (see Section 4), are in good agreement. However, the experimental results are close to a straight line while the box model predicts a slope (velocity) which slightly decreases with time. The box model using $\overline{h}$ gives poorer results. For this case $Fr = 0.9$ and $Fr^* = 1.4$.

In the above dimensionless graphs, $y = 1$ indicates when the length of the currents is first entirely within the valley.

5.2. Experiments with viscous effects

In experiments 12 and 13, in which the front of the current was recorded over a length greater than 1.5 m, viscous effects appear. We show in Fig. 10 the evolution of y with τ for these two experiments. Both experiments had the same g' but different values of H_0 (see Table 1). The experimental results are shown by open squares. The results from the box model are shown by the continuous line (when h is used as the characteristic depth) and, by dots (when $\overline{h}$ is instead used). Experiment 10 with $H_0 = 0$ m (Fig. 10a) shows a transition around $\tau = 50$, and $y = 35$, corresponding to $t = 40.5$ s and $X = 4.55$ m. The associated estimate of the Reynolds number given in the Appendix is 0.8. Experiment 11 for which $H_0 = 0.035$ m (Fig. 10b) does not show a transition. Estimating the Reynolds number as before we predict a transition to the viscous regime at $\tau \geq 44$ which is outside the domain of the experimental results.

5.3. Effect of the depth of the valley a

Because the box model gives results in good agreement with the experiments, it is interesting to use it to examine the effect of the slope of the valley. Because the scaling used previously involves a, it is more convenient to work with the variables X and t rather than y and τ. We considered a typical case where the ratio of the density of the current to that of the ambient fluid is 1.08. We used a fixed volume V of current (calculated using Eq. (13) with $H_0 = 0.06$ m and $a = 0.06$ m). We then

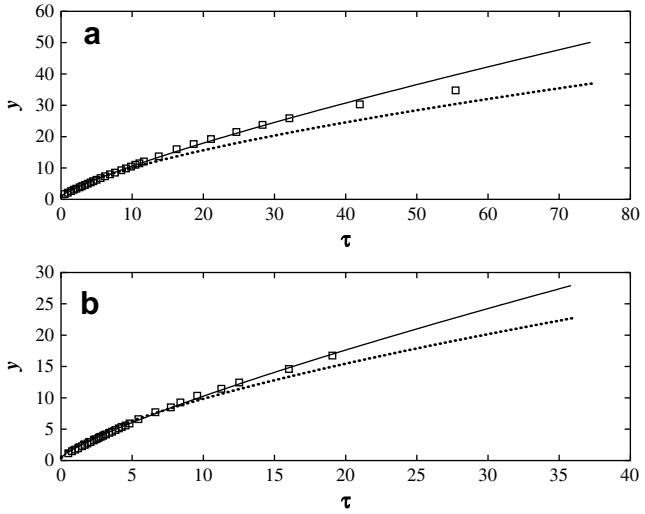

Fig. 10. The non-dimensional position of the head of the gravity current against non-dimensional time for experiments 10 (Fig. 10a) and 11 (Fig. 10b). The experimental data are shown by the open squares. The results for the box model using h are shown by the solid line, and the results using $\overline{h}$ are shown by the dotted line.

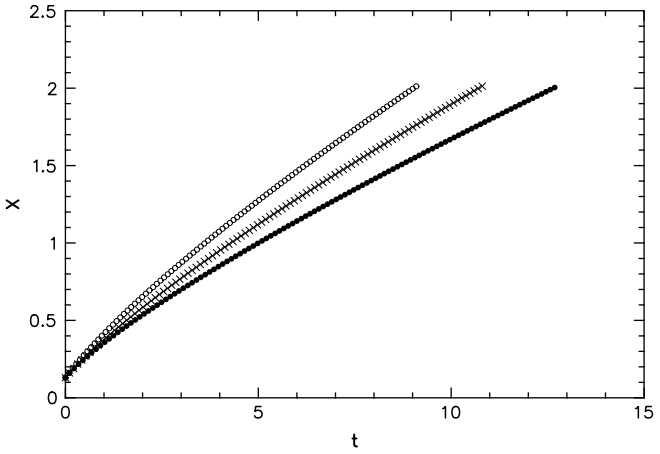

Fig. 11. The variation of the distance to the head of the current X with time t for different values of a but fixed volume of the currents. The results are shown by small filled circles for the case with $a = 0.03$ m, by crosses for the case with $a = 0.06$ m, and by small open circles for the case with $a = 0.12$ m.

chose a equal to 0.03, 0.06 and 0.12 m, with corresponding angle of the flanks of the valley to the horizontal 12, 23 and 41 degrees, and determined H_0 from V. Equations (19) and (21) were then integrated. The results in Fig. 11 show that, for equal volume currents, the steeper the flanks of the V-shaped valley the faster the flow.

6. Conclusions

We have conducted a series of 11 experiments in which a volume of saline solution was instantaneously released into water in a tank with vertical side walls and a V-shaped bottom. The presence of the V-shaped bottom profoundly alters the flow of a gravity current from the lock whether the tank into which it flows is empty (where the ambient fluid is air), or filled with water.

The gravity current propagates with a parabolic head. The radius of curvature is proportional to the initial depth of the current, and remains nearly constant during the propagation, for each current that we studied. The side profile is irregular, without the distinctive head of gravity currents in a tank with a flat bottom. The experiments show that the results for the speed of the head against time, for a given initial depth of fluid but different densities, collapse onto a single curve when appropriate scaled variables are used.

The position of the head as a function of time is captured with satisfactory accuracy by a box model with the speed of the front given by a Froude number condition based on the depth from the top of the current to the bottom of the valley. Calculations using a box model with a Froude number calculated using an averaged depth give less accurate results. We estimate the onset of significant viscous effects by calculating the Reynolds number when deviations between the box model results and those of the experiments become noticeable. This only occurs for experiment 10. Our estimate of the Reynolds number when viscous effects occur is similar to that estimated by Bonnecaze et al. [30]. The width of the currents is also well predicted by the box model.

The presence of the valley results in three major differences in the gravity current compared to that flowing along a flat boundary. First the front of the current is straight in the flat bottom case whereas it is curved in V-shaped case. Second, for sufficiently large time t, the velocity of the current in the V-shaped valley varies as $t^{-1/5}$ compared to $t^{-1/3}$ in the flat bottom case. Third the width of the current is constant in the flat bottom case whereas, in the V-shaped case, it decreases with time t according to $t^{-2/5}$.

Because of the good agreement between the results of the box model and the experiments, we have used the box model to predict the effect of changing the slope of the valley. The result is that for equal volume currents, the steeper the valley the faster the flow.

The results presented suggest further work for the future. A different sized V-shaped container and even a different shaped container altogether may produce novel phenomena. Finally we have already begun to consider the effects due to particle-laden flows driven by a dilute concentration of particles in the fluid.

Acknowledgements

We thank R.T. Bonnecaze, M.A. Hallworth, A.J. Hogg, P.F. Linden, D. Takagi and D. Vella for helpful comments on a first draft of this paper. The research of HEH is supported by both a Royal Society Wolfson Merit Award and the Australian Research Council. The research of JJM is supported by the Australian Research Council. CM acknowledges financial support from ARC grant DP0449979.

A. Critical Reynolds number

Inertial forces do not dominate the dynamics of a gravity current indefinitely. As a current lengthens, the viscous forces acting at the bottom of the current over a rigid boundary become more important. The conditions for a transition from inertial to viscous dominated propagation was described for flat bottom boundaries by Huppert [31] and Bonnecaze et al. [30] in terms of a critical Reynolds number. Here we estimate the onset of viscous effects for gravity currents flowing entirely in a V-shaped valley following the same argument. We first estimate the Reynolds number by taking the ratio of the inertial forces F_i to the viscous forces F_v. The transition occurs when Re is $O(1)$.

The inertial forces can then be estimated as

$$F_i \sim \rho_c \dot{X}^2 \left(\frac{h^2 W}{2a}\right), \tag{A1}$$

and the viscous forces as

$$F_v \sim 2s\mu X \left(\frac{\dot{X}}{h/2}\right), \tag{A2}$$

where s is the distance from the bottom of the valley up to the point leveled with the current surface. The velocity gradient is estimated as $\dot{X}/(h/2)$ since the depth varies between h in the centre of the tank and zero at the edge. From the ratio of the inertial to the viscous forces, we find that the Reynolds number is given by

$$Re = \frac{h^2 \dot{X}}{\nu X}\left(\frac{W \sin\theta}{8a}\right), \tag{A3}$$

where θ is the angle of the slope of the valley to the horizontal. Using the expressions for $X, \dot{X}$, and h in terms of X appropriate to the case when the current is entirely in the V-shaped part of the tank (see Section 4), gives

$$Re = \frac{V \sin\theta}{5\nu}\left(\frac{4}{5\zeta}\right)^{4/5} t^{-9/5}. \tag{A4}$$

where

$$\zeta = Fr\left(\frac{2ag'^2 V}{W}\right)^{1/4}. \tag{A5}$$

From the upper frame of Fig. 8, the box model results begin to deviate strongly from the experiments when $\tau \sim 50$ or $t \sim 40.5$ s. If this value of t is assumed to reflect the time for the transition from inertial to viscous flow we find $Re \sim 0.8$ after substitution

into Eqs. (A4) and (A5) using the parameters of experiment 10. This value is slightly smaller than that of Huppert [31] and Bonnecaze et al. [30] who estimated $Re \sim 2$, for experiments in a flat-bottomed tank.

References

[1] J.E. Simpson, Gravity Currents in the Environment and Laboratory, Cambridge University Press, 1997, p. 243.
[2] J.E. Simpson, Gravity currents in the laboratory, atmosphere and ocean, Ann. Rev. Fluid Mech. 14 (1982) 213–234.
[3] T.H. Ellison, J.S. Turner, Turbulent entrainment in stratified flows, J. Fluid Mech. 6 (1959) 423–448.
[4] R.E. Britter, P.F. Linden, The motion of the front of a gravity current travelling down an incline, J. Fluid Mech. 99 (1980) 531–543.
[5] P. Beghin, E.J. Hopfinger, R.E. Britter, Gravitational convection from instantaneous sources on inclined boundaries, J. Fluid Mech. 107 (1981) 407–422.
[6] D.M. Webber, S.J. Jones, D. Martin, A model of the motion of a heavy gas cloud released on a uniform slope in calm conditions, J. Hazard Mater. 33 (1) (1993) 101–122.
[7] J.J. Monaghan, R.A.F. Cas, A.M. Kos, M.A. Hallworth, Gravity currents descending a ramp in a stratified tank, J. Fluid Mech. 379 (1999) 39–70.
[8] J.J. Monaghan, Gravity currents interaction with interfaces, Ann. Rev. Fluid Mech. 39 (2007) 245–261.
[9] M.G. Wells, J.S. Wettlaufer, The long-term circulation driven by density currents in a two-layer stratified basin, J. Fluid Mech. 572 (2007) 37–58.
[10] A.N. Ross, S.B. Dalziel, P.F. Linden, Axisymmetric gravity currents on a cone, J. Fluid Mech. 565 (2006) 227–253.
[11] F.M. Henderson, Open Channel Flow, Macmillan, New York, 1966.
[12] J.P. Antenucci, J.D. Brookes, M.R. Hipsey, A simple model for quantifying Cryptosporidium transport, dilution and potential risk in reservoirs, J. Am Water Works Assoc. 97 (2005) 86–93.
[13] G.M. Keevil, J. Peakall, J. Best, K.J. Amos, Flow structure in sinuous submarine channels: velocity and turbulence structure of an experimental channel, Mar. Geol. 229 (2006) 241–257.
[14] M.A. Islam, J. Imran, Experimental modeling of gravity underflow in a sinuous submerged channel, J. Geophys. Res. 113 (2008). doi:10.1029/2007JC004292 C07041.
[15] J. Kampf, Impact of multiple submarine channel on the descent of dense water at high latitudes, J. Geophys. Res. 105 (2000) 8753–8773.
[16] P.A. Davies, A.K. Wåhlin, Y. Guo, Laboratory and analytical model studies of the Faroe bank channel deep-water outflow, J. Phys. Oceano. 36 (2005) 1348–1364.
[17] A.K. Wåhlin, E. Darelius, C. Cenedese, G.F. Lane-Serff, Laboratory observations of enhanced entrainment in dense overflows in the presence of submarine canyons and ridges, Deep Sea Res. 55 (2008) 737–750.
[18] E. Darelius, Topographic steering of dense overflows: laboratory experiments with V-shaped ridges and canyons, Deep Sea Res. 1 (155) (2008) 1021–1034.
[19] D. Takagi, H.E. Huppert, The effect of confining boundaries on viscous gravity currents, J. Fluid Mech. 577 (2007) 495–505.
[20] D. Takagi, H.E. Huppert, Viscous gravity currents inside confining channels and fractures, Phys. Fluids 20 (2008) 1–8 023104.
[21] M.I. Cantero, J.R. Lee, S. Balachandar, M.H. Garcia, On the front velocity of gravity currents, J. Fluid Mech. 586 (2007) 1–39.
[22] B.L. White, K.R. Helfrich, Gravity currents and internal waves in a stratified fluid, J. Fluid Mech. 616 (2008) 327–356.
[23] T. van Kármán, The engineer grapples with non-linear problems, Bull. Am. Math. Soc. 46 (1940) 615–683.
[24] T.B. Benjamin, Gravity currents and related phenomena, J. Fluid Mech. 31 (1968) 209–248.
[25] H.E. Huppert, J.E. Simpson, The slumping of gravity currents, J. Fluid Mech. 99 (1980) 785–799.
[26] J.O. Shin, S.B. Dalziel, P.F. Linden, Gravity currents produced by lock exchange, J. Fluid Mech. 521 (2004) 1–34.
[27] B.M. Marino, L.P. Thomas, P.F. Linden, The front condition for gravity currents, J. Fluid Mech. 536 (2005) 49–78.
[28] J.C. Martin, W.J. Moyce, An experimental study of the collapse of liquid columns on a rigid horizontal plane, Philos. Trans. R. Soc. 244 (1952) 312–324.
[29] G.B. Whitham, Linear and Nonlinear Waves, Wiley Press, New York, 1974.
[30] R.T. Bonnecaze, H.E. Huppert, J.R. Lister, Particle-driven gravity currents, J. Fluid Mech. 250 (1993) 339–369.
[31] H.E. Huppert, The propagation of two-dimensional and axisymmetric viscous gravity currents over a rigid horizontal surface, J. Fluid Mech. 121 (1982) 43–58.